



## The magmatic plumbing system beneath Santiaguito Volcano, Guatemala

Jeannie A.J. Scott <sup>a,\*</sup>, Tamsin A. Mather <sup>a</sup>, David M. Pyle <sup>a</sup>, William I. Rose <sup>b</sup>, Gustavo Chigna <sup>c</sup>

<sup>a</sup> Department of Earth Sciences, University of Oxford, South Parks Road, Oxford, OX1 3AN, UK

<sup>b</sup> Department of Geological and Mining Engineering and Sciences, Michigan Technological University, 1400 Townsend Drive, Houghton, Michigan 49931, USA

<sup>c</sup> Instituto Nacional de Sismología, Vulcanología, Meteorología, e Hidrología (INSIVUMEH), 7a Avenue 14-57, Zone 13, Guatemala City, Guatemala

### ARTICLE INFO

#### Article history:

Received 9 September 2011

Accepted 16 May 2012

Available online 2 June 2012

#### Keywords:

Santiaguito

Dome

Magmatic plumbing system

Magma storage

Ascent path

### ABSTRACT

The silicic dome complex of Santiaguito, Guatemala, has exhibited continuous extrusive activity for 90 years. Despite its longevity, remarkably little is known about the magmatic plumbing system beneath Santiaguito. Here, we use petrological analyses of lava samples to define this plumbing system, from storage in the lower to mid-crust through to extrusion onto the surface. Magmatic storage conditions are constrained using amphibole and plagioclase phenocrysts; ascent processes are examined using the breakdown rims of amphibole phenocrysts and the texture and composition of groundmass, while shallow processes are revealed by the alteration of titanomagnetites and matrix glass. Santiaguito magmas contain amphiboles that formed from ~24 km to ~12 km beneath the surface, with temperatures of ~940 to ~980 °C, and  $f_{O_2}$  of NNO +0.4 to NNO +1.2. Amphibole breakdown rims suggest that during the final phases of ascent, magma may rise from ~12 km (the limit of amphibole stability) relatively rapidly (~27 to ~84 m h<sup>-1</sup>). We infer from the texture of the groundmass that melt rigidifies prior to extrusion – a finding that may have important consequences for conduit dynamics.

© 2012 Elsevier B.V. All rights reserved.

### 1. Introduction

The silicic lava dome complex of Santiaguito, Guatemala, lies within a crater formed during the cataclysmic eruption of its parent stratocone, Santa Maria, in 1902 (Fig. 1) (Rose, 1972). Activity at Santiaguito has been continuous since its inception in 1922 and is characterized by small to moderate explosions of steam, gas, and ash, small pyroclastic flows and rockfalls, frequent lahars during Guatemala's wet season, and effusion of blocky lava domes and flows. Lava flows have become increasingly dominant since the 1960s, with some extending over ~3 km from the vent (Stoiber and Rose, 1968; Rose, 1972; Harris et al., 2003; Bluth and Rose, 2004; Escobar Wolf et al., 2010; Santa Maria Volcano Observatory written records).

Understanding the long-term behavior and consequent hazards of persistent dome-forming systems like Santiaguito requires an understanding of the storage and ascent processes of magma within those systems (e.g., Cashman and Blundy, 2000; Rutherford and Devine, 2003; Clarke et al., 2007). The temperature and pressure within magma chambers and rates of magma ascent and extrusion can inform models of supply and eruption dynamics, the interpretation of seismic, petrologic, and emissions data, and ultimately improve hazard assessment (e.g., Rutherford and Hill, 1993; Hammer

et al., 2000). These processes have been constrained at other, better-studied dome-forming systems using a variety of geochemical and petrological techniques (e.g., ascent rate of Mount St Helens magma from amphibole rim widths, Rutherford and Hill, 1993; magma chamber conditions from the stability of the mineral assemblage at Soufrière Hills, Barclay et al., 1998; ascent and extrusion processes from groundmass texture at Merapi, Hammer et al., 2000). In this paper, we combine key information extracted from the composition and decay of amphibole phenocrysts, the texture of plagioclase crystals, the texture and geochemistry of groundmass, and the oxidation of titanomagnetites to develop a preliminary picture of the magmatic plumbing beneath Santiaguito.

### 2. Methods

Forty-one rock samples were obtained from Santiaguito, representing many of the lava units and ranging in age from the 1920s to 2002 (Supplementary Information Table A). Our results are based on scanning electron microscope (EDS) and electron microprobe (WDS) analyses of multiple polished thin sections (Supplementary Information Table B), examination of back-scattered electron (BSE) images, and crystal size distribution analysis of plagioclase phenocrysts and microlites (carried out using ImageJ and CSDCorrections 1.3.8; Higgins, 2000). The degree of oxidation in titanomagnetites was classified using the scheme of Haggerty (1991) (Supplementary Information Table C). A full methodology is provided in electronic Appendix A.

\* Corresponding author. Tel.: +44 1865 272000; fax: +44 1865 272072.

E-mail addresses: [jeannie.scott@earth.ox.ac.uk](mailto:jeannie.scott@earth.ox.ac.uk) (J.A.J. Scott),

[tamsin.mather@earth.ox.ac.uk](mailto:tamsin.mather@earth.ox.ac.uk) (T.A. Mather), [david.pyle@earth.ox.ac.uk](mailto:david.pyle@earth.ox.ac.uk) (D.M. Pyle), [raman@mtu.edu](mailto:raman@mtu.edu) (W.I. Rose).

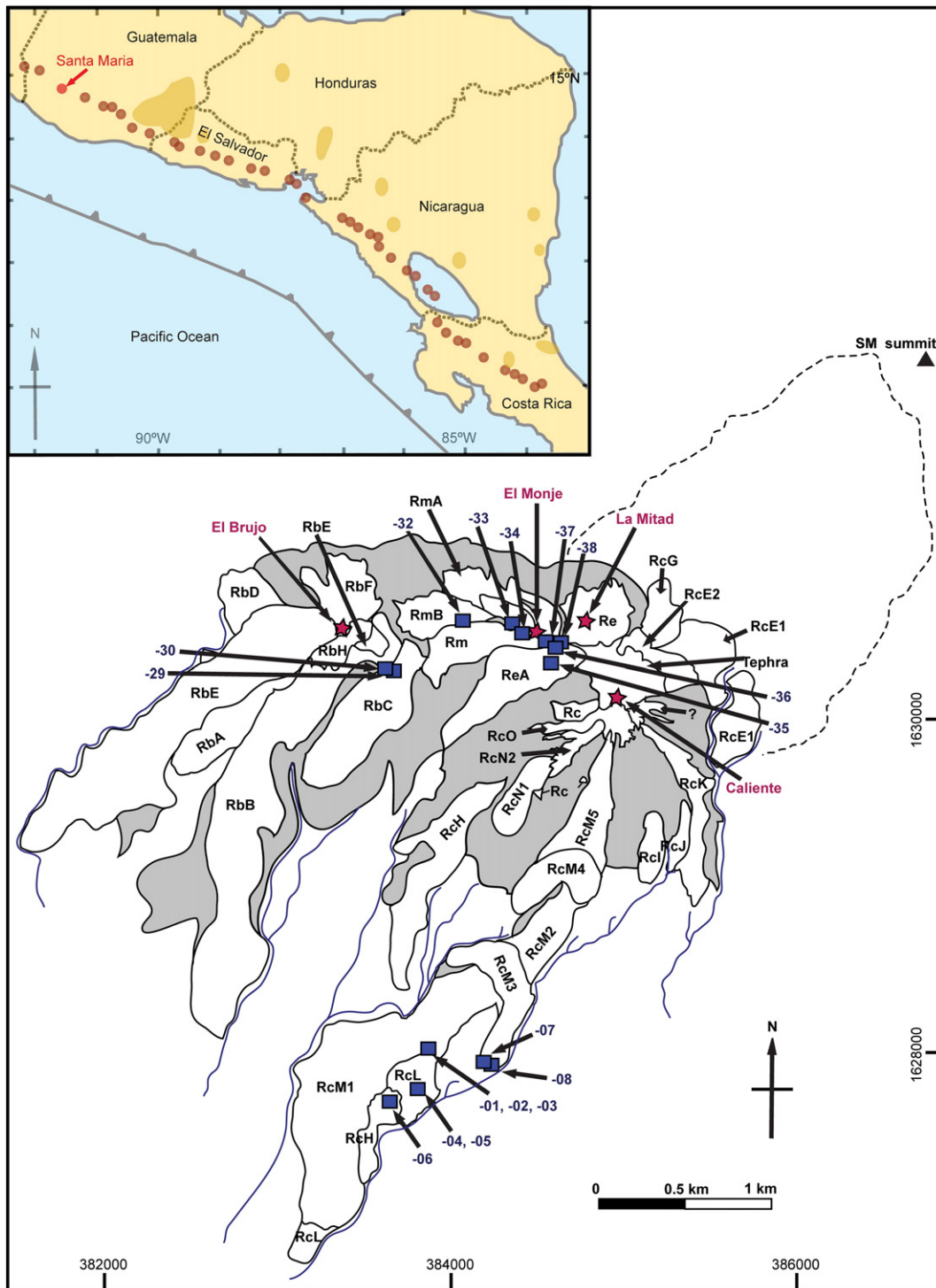


**Fig. 1.** Map of the Santiaguito complex, modified from Escobar Wolf et al. (2010), showing the four vents (Caliente, La Mitad, El Monje, El Brujo) and lava dome and flow units. Unit nomenclature uses the second letter to designate the source vent: Rc for Caliente, Re for La Mitad, Rm for El Monje, and Rb for El Brujo. Shaded areas are talus and fluvial deposits; the heavy blue lines are rivers and streams. The locations of samples obtained during a 2009 field trip are shown; only the last two digits from each sample name is used here (Supplementary Information Table A lists all samples). Note that many older Santiaguito units are now buried. The coordinate system is GTM (Guatemala Transverse Mercator). Inset: the Central American volcanic arc; circles show the location of arc front volcanoes, shaded patches show regions of back-arc activity (from Carr et al., 1990; Walker et al., 2000; Cáceres et al., 2005).

### 3. Results

#### 3.1. Phenocrysts

Santiaguito dome rocks are porphyritic andesites and dacites with phenocrysts of plagioclase, two pyroxenes, titanomagnetite, and amphibole; apatite and pyrrhotite are common accessory minerals, while

crystalline silica, most likely cristobalite, is a scarce accessory mineral in 25 samples (Supplementary Information Table D).

The phenocryst assemblage is dominated by normally zoned plagioclase (20–28 modal%, with cores typically An<sub>50–60</sub> and rims of An<sub>40–50</sub>), although reverse zoning, sieved cores, and dusty zones or patches are sometimes present. Many plagioclase crystals are broken, with jagged edges and fractures; the largest intact crystals are typically <1.5 mm

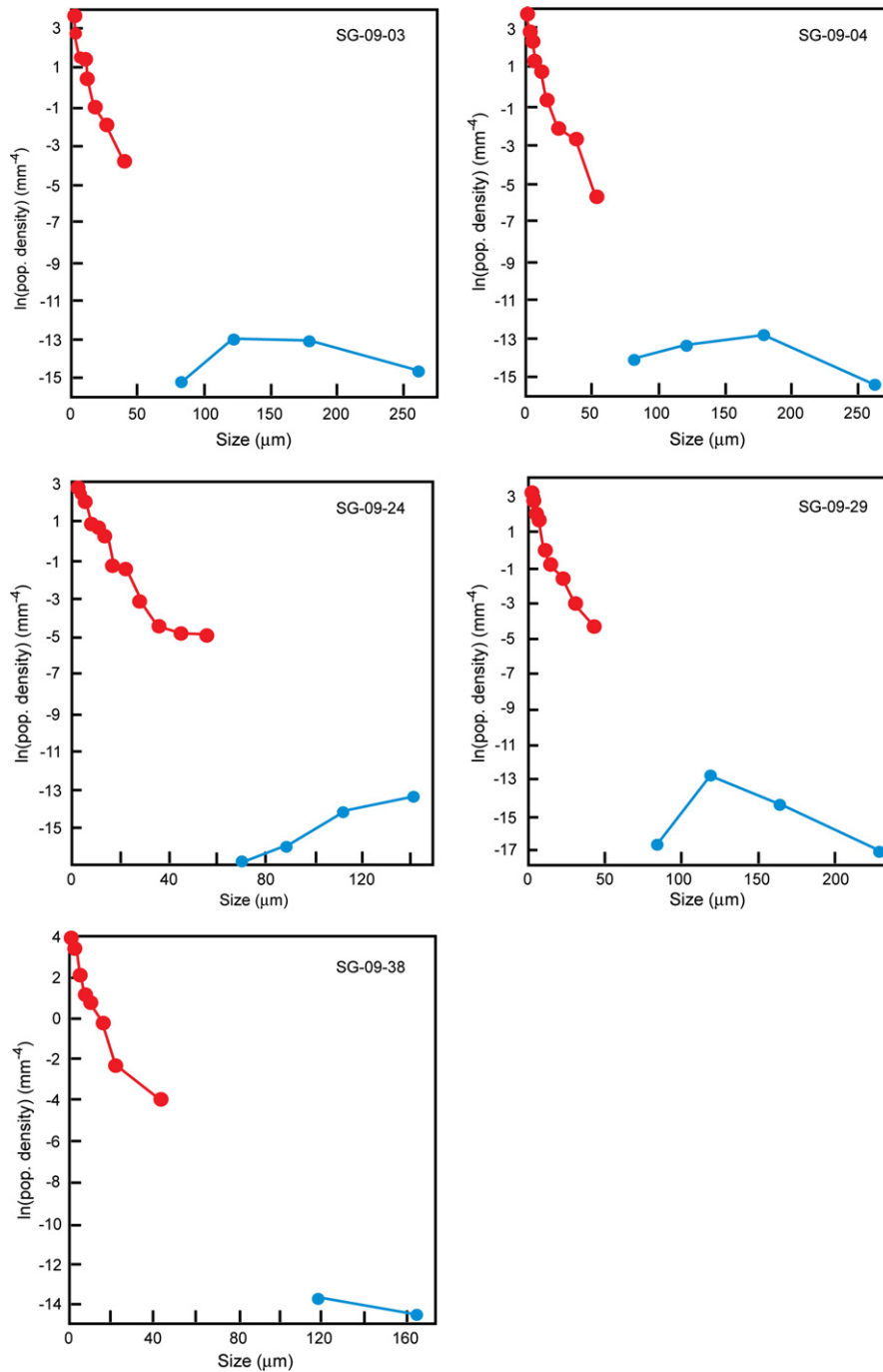


**Fig. 2.** Crystal size distribution plots for plagioclase microlites (red, <60 micrometers) and phenocrysts (blue, >60 micrometers) (obtained using CSDCorrections; Higgins, 2000); the gap between these two distinct populations is a natural characteristic of the data set. Due to the very considerable size differences between microlites and the majority of the phenocryst population, only the smallest phenocrysts could be included. SG-09-03 and SG-09-04 include phenocrysts up to 20000  $\mu\text{m}^2$ ; SG-09-24, SG-09-29, and SG-09-38 include phenocrysts up to 10,000  $\mu\text{m}^2$ .

long; size distributions of smaller plagioclase phenocrysts are included in Fig. 2. Pyroxenes (mostly enstatite, with some augite) account for <4 modal% (Bardintzeff et al., 1980); they are typically <500  $\mu\text{m}$  diameter. Titanomagnetites <350  $\mu\text{m}$  diameter account for ~1 modal% (Bardintzeff et al., 1980). The extent of titanomagnetite oxidation, evidenced by “trellis” lamellae (Fig. 3b–f), varies between samples – this variability is discussed further in Section 4.3.2.

The abundance and condition of amphibole phenocrysts varies greatly between samples (Supplementary Information Table D). Where most abundant, amphiboles up to ~500  $\mu\text{m}$  long account for <4 modal%; where least abundant, they account for <1 modal%. Different Santiaguito samples contain amphiboles at different stages of decomposition

(Supplementary Information Figure A), from thin rims (Fig. 4a) to complete breakdown to plagioclase–pyroxene–titanomagnetite clusters (Fig. 4f). Such clusters are present, sometimes common, in at least 30 of our samples. In samples extruded from 2000 to 2002, amphibole is present only as occasional clusters of decomposition products. Where amphiboles were preserved with only partial decay rims, the widths of these rims were used to estimate magma ascent rates using the experimental calibration of Rutherford and Hill (1993). We estimate maximum ascent rates of 27–84  $\text{m h}^{-1}$  for Santiaguito (Table 1, method is detailed in table footnotes; results are discussed in Section 4.2.1).

The remnant cores of Santiaguito amphiboles are calcic, with ~11 to ~15 wt.%  $\text{Al}_2\text{O}_3$ , typically <3 wt.%  $\text{Na}_2\text{O}$ , and  $\text{K}_2\text{O}$  present only in

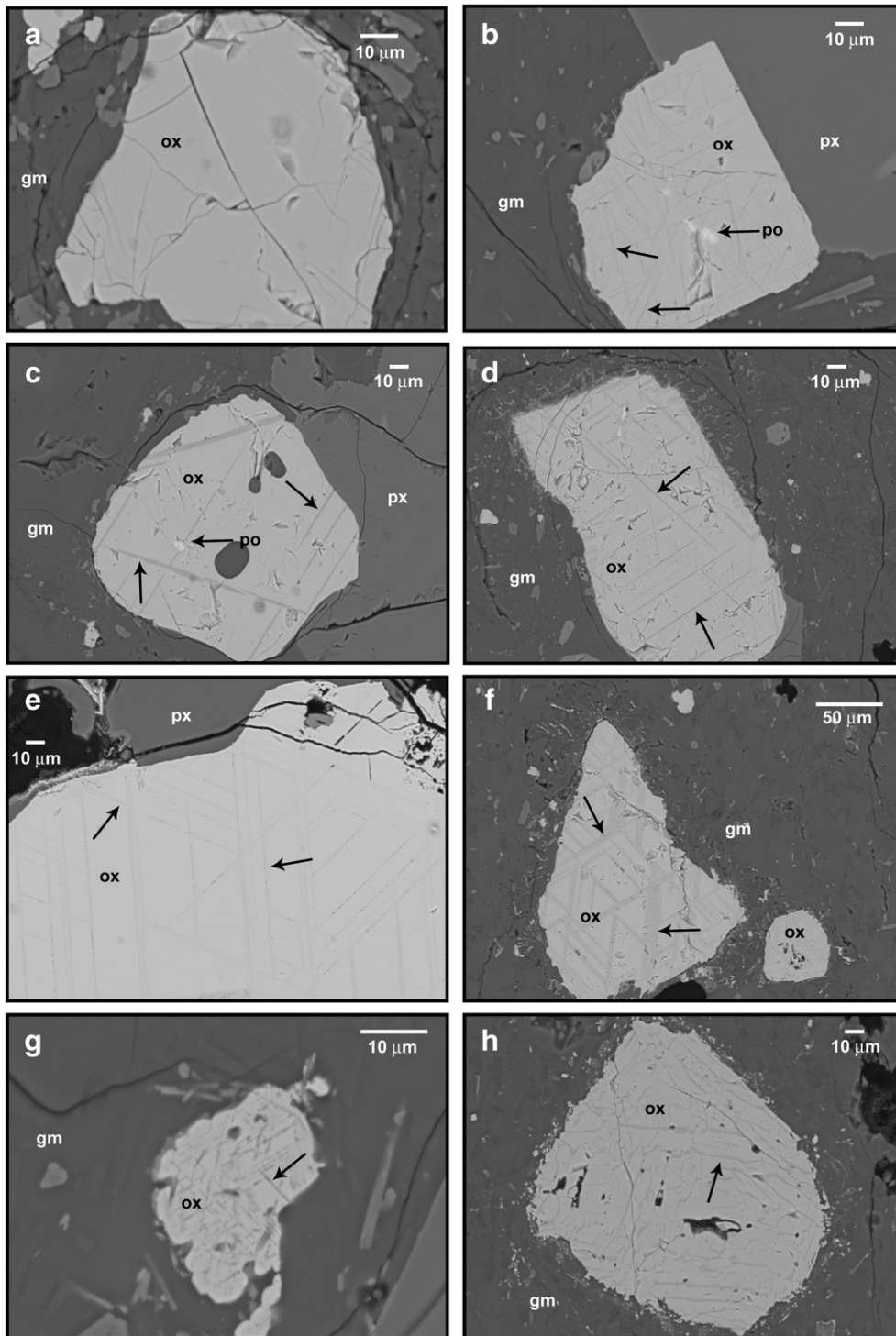


**Fig. 3.** The stages of oxyexsolution in Santiaguito titanomagnetites (the stages are defined in Supplementary Information Table C and Haggerty, 1991). (a) An example of early stage C2 shows a few thin lamellae forming on the edges of the crystal; (b) stage C3, with thin lamellae extending across the whole crystal (shown by the black arrows); (c) stage C3 with some thicker lamellae. The very thick streaks with sides which are not parallel to each other are sandwich laths, not part of the trellis texture; (d) lamellae thicken further as oxyexsolution progresses, and tiny crystals have formed within some lamellae – this is early stage C4. (e) A close-up of C4 lamellae containing tiny spinel crystals; (f) thicker lamellae, with larger spinels indicating more advanced C4; (g) advanced oxyexsolution occurs in very small microlites too – this is too small for analysis, so its stage cannot be determined. (h) A rare C7 – the lamellae are extremely distorted, destroying the trellis texture. All are BSE images with very low brightness and contrast.

trace amounts (Table 2). Transects across these cores show the concentration of temperature-dependent elements (Ti, Na, K, Ca) and Cl (which may change as fresh magma is introduced into the system) fluctuate, suggesting variable conditions during their growth (Supplementary Information Figure B). The Holland and Blundy (1994) plagioclase–amphibole geothermometer suggests temperatures beneath Santiaguito range from ~840 to ~950 °C ( $\pm 40$  °C), while the more

recent Ridolfi et al. (2010) geothermometer (which does not assume amphibole and plagioclase are in equilibrium) yields a smaller range of estimates, from 938 to 984 °C ( $\pm 22$  °C) (Fig. 5). The Ridolfi et al. (2010) technique also provides an estimate of oxygen fugacity beneath Santiaguito of  $\log f_{O_2} - 9.3$  to  $-10.3$  ( $\pm 0.4$  log units; equal to NNO + 0.4 to +1.2) (Fig. 6b), and dissolved magmatic H<sub>2</sub>O content of 5–7% (Fig. 6c).

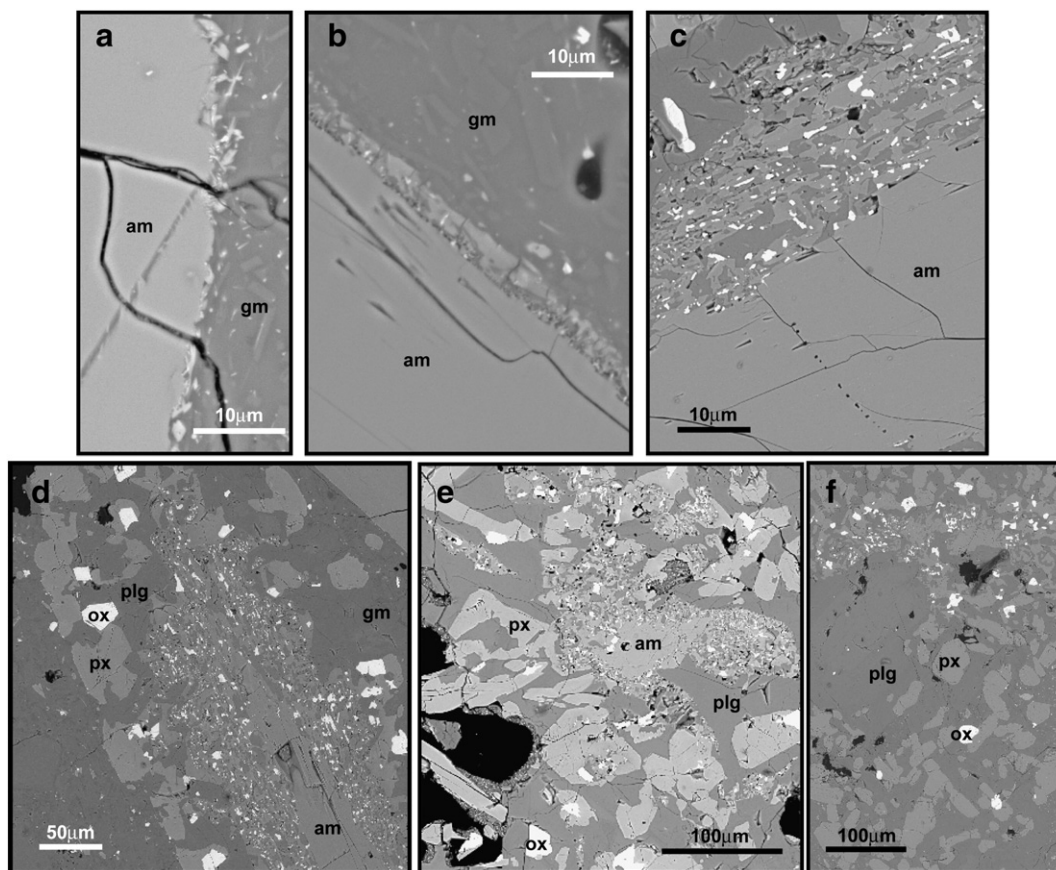


**Fig. 4.** BSE images of amphiboles (am) from different Santiaguito samples showing the progression of granular breakdown. It begins with 'grazing' of the smooth crystal edge (a), producing tiny fragments of plagioclase (plg), pyroxene (px), and titanomagnetite (ox) (b); these fragments grow and coalesce as the decay front migrates inward (c, d); as breakdown nears completion, the rim disappears, leaving a cluster of rounded pyroxenes and titanomagnetites set in plagioclase (e, f). From the following samples: (a) 1004-67, (b) 1104-67, (c) SG-09-33, (d) SG-09-30, (e) SG-09-30, (f) SG-09-03.

Amphibole composition was also used to estimate the depth at which phenocrysts form beneath Santiaguito. The total Al content ( $Al^T$ , recalculated to 23 O atoms) of a selection of amphiboles from different samples was used with Johnson and Rutherford's (1989) barometer, and the results suggest there is a continuous region of amphibole crystallization between ~440 and ~630 MPa ( $\pm 50$  MPa), equivalent to ~17 to ~24 km beneath Santiaguito. The more recent geobarometer of Ridolfi et al. (2010) improves upon the Johnson and Rutherford (1989) method by incorporating complete major element geochemistry of amphiboles; these results (Fig. 5) also imply an extensive, continuous amphibole crystallization zone from ~330 to ~615 MPa ( $\pm 50$  MPa), or ~12 to ~24 km ( $\pm 2$  km) (see Section 4.1.1).

### 3.2. Groundmass

The groundmass of Santiaguito lavas consists of 67–81 vol% glass, 11–22% plagioclase microlites, 1–6% mafic microlites, and 0–8% vesicles (Table 3). Plagioclase microlites are mostly tabular, with only a few swallowtail or hopper crystals present in typical samples (Fig. 7). Their number density ( $N_A$ ) ranges from ~4000 to ~20,000  $mm^{-2}$ ; their average aspect ratio is 1.9–3.6 (Table 3). Mafic microlites are generally far smaller than plagioclase, although they often have a higher number density ( $N_A$  ranges from ~1000 to ~46,000  $mm^{-2}$ ; Table 3; Section 4.2.2). Pyroxenes are often feathery and sometimes rimmed by extremely small ( $<0.5 \mu m$ ) specks of BSE-bright material (presumably Fe oxides) typical of incipient, progressing crystallization (Fig. 7). A few larger oxide microlites show evidence of oxyexsolution, but most are far too small ( $<0.1 \mu m$ ). Vesicles are usually small ( $<10 \mu m$  diameter), concentrated in clusters or trains, with some preservation of melt films (Fig. 7d,e). Microlites are

geochemically indistinguishable from plagioclase, enstatite, and titanomagnetite phenocrysts (full analyses are included in Supplementary Information Table E). BSE images (Fig. 7) and element mapping (Supplementary Information Figure C) show a very thin ( $<2 \mu m$ ) Na-rich rim around some plagioclase microlites, but the vast majority appear geochemically homogeneous.

72% to 87% of the solid groundmass area consists of heterogeneous dacitic, trachytic, and rhyolitic glass (Table 3; Fig. 8). The matrix glass of many Santiaguito samples has undergone heterogeneous and progressive decomposition to a silica-rich phase and an alkali-rich phase (described in Fig. 7; discussed in Section 4.3.1). Our BSE images (Fig. 7) suggest that decaying glass develops a sub-micron-scale web-like texture before separating into larger ( $<5 \mu m$ ), anhedral patches of the final decay products. This differs somewhat from the devitrification processes observed elsewhere, such as the segregation of glass phases and the growth of microlites (e.g., Mount St. Helens, USA, Cashman, 1992; Merapi, Indonesia, Hammer et al., 2000).

## 4. Discussion

### 4.1. Magma storage

#### 4.1.1. Amphibole thermobarometry

Since amphibole phenocrysts form under hydrous, high-pressure conditions, they provide important constraints on the temperature and pressure experienced by stored magma prior to ascent (e.g., Johnson and Rutherford, 1989; Ridolfi et al., 2010). The little geochemical variation between the preserved cores of Santiaguito amphiboles (Table 2, Fig. 5) suggests that all formed under similar conditions from a similar

**Table 1**

Average amphibole rim widths (number; range), ascent rates, and total ascent times for all Santiaguito samples bearing multiple, preserved amphibole phenocrysts.

Sample	Lava unit	Bulk SiO <sub>2</sub> (wt.%) <sup>a</sup>	Avg. rim width (μm) <sup>b</sup>	Ascent rate (m h <sup>-1</sup> ) <sup>c</sup>	Ascent duration <sup>d</sup>	
					Hours	Days
SG-09-06	RcH (1986–89)	63.08	5.8 (3; 5–6)	76	151	6
SG-09-23	<1936	64.91	42.4 (4; 35–51)	27	432	18
SG-09-24	<1936	65.92	31.1 (3; 24–36)	37	312	13
SG-09-29	RbC (1963–66)	63.78	20.1 (3; 15–23)	52	221	9
SG-09-32	RmB (1956–58)	64.10	17.7 (5; 13–21)	56	206	9
SG-09-33	RmA (1952?)	64.52	20.9 (3; 15–27)	50	230	10
SG-09-37	ReA (1940s)	64.26	14.2 (6; 10–20)	61	190	8
915-67	RcD (1927–29)	–	5.9 (5; 4–7)	76	151	6
1001-67	RcD (1927–29)	–	11.8 (6; 7–16)	67	173	7
1004-67	RcA (1932–34)	65.74	3.6 (3; 2–5)	84	137	6
1104-67	RcB (1929–34)	65.56	5.3 (4; 2–9)	77	149	6
1120-67	Rb (1958–??)	–	9.5 (6; 8–12)	69	168	7
1121-67	Rb (1958–??)	–	11.7 (2; 10–13)	67	173	7
1234.67	RcA (1932–34)	–	4.4 (3; 4–5)	80	144	6
1320-67	Re (1939?–42?)	–	5.5 (2; 5–6)	77	149	6
1612	Rm (1947–52?)	–	20.8 (2; 19–22)	50	228	10
1619	bomb (1968)	–	12.9 (4; 10–21)	65	178	7
2001-69	Re (1939?–42?)	–	18.0 (3; 9–24)	55	211	9
2002-69	Re (1939?–42?)	–	5.8 (8; 4–9)	76	151	6
2003-69	Re (1939?–42?)	64.88	16.3 (3; 13–22)	59	194	8
2004-69	Re (1939?–42?)	–	17.2 (5; 10–23)	57	201	8

<sup>a</sup> SiO<sub>2</sub> content for archived samples are from Rose (1972) and Rose (1987); bulk analyses are not available for all archived samples. SiO<sub>2</sub> content for samples collected in 2009 is from Scott et al. (unpublished data).

<sup>b</sup> Amphiboles without substantial preserved cores were excluded; this ensures that rim widths represent the extent of crystal decay, and not the angle at which the rock was sectioned.

<sup>c</sup> Rim widths measured from BSE images were used to obtain ascent rates using Fig. 6 of Rutherford and Hill (1993), assuming continuous, isothermal ascent at ~900 °C best represents conditions at Santiaguito.

<sup>d</sup> Santiaguito amphibole phenocrysts become unstable at ~12 km depth. Amphibole decay is kinetically inhibited within a few hundred meters of the surface (Rutherford and Hill, 1993; Browne and Gardner, 2006). Therefore, conduit length was estimated at 11.5 km.

parental magma. There is as much variability in thermobarometric data from amphiboles within the same thin section as there is between thin sections or lava units (Fig. 5a), and we find no correlation between thermobarometric data and the degree of amphibole breakdown, although

**Table 2**

Selected Santiaguito amphibole analyses (wt.%, prior to recalculation to 23 oxygens); WDS analysis was used for SG-09-37, EDS for all others. SG-09-37 includes analyses from four different amphibole phenocrysts: (a), (b), (c), and (d); SG-09-37, 1104-67, and 1612 include analyses of different points within the same phenocryst.

Sample	SiO <sub>2</sub>	TiO <sub>2</sub>	Al <sub>2</sub> O <sub>3</sub>	FeO	MgO	CaO	Na <sub>2</sub> O	K <sub>2</sub> O	Total
SG-09-06	43.1	2.9	11.9	12.8	14.5	11.2	3.0	0.4	99.9
SG-09-29	43.4	2.5	12.1	12.6	14.7	11.4	2.4	0.4	99.8
SG-09-32	42.7	2.1	12.5	13.8	13.8	11.1	2.7	0.4	99.3
SG-09-37 (a)	40.7	2.3	12.7	13.0	14.0	11.2	2.4	0.4	96.7
SG-09-37 (a)	41.5	2.7	12.6	13.7	13.1	11.5	2.4	0.4	98.2
SG-09-37 (a)	41.3	2.3	14.3	13.4	13.0	11.3	2.4	0.4	98.6
SG-09-37 (b)	42.1	2.5	12.1	14.3	13.8	11.1	2.5	0.4	99.0
SG-09-37 (b)	42.4	2.6	12.3	14.1	13.4	11.3	2.4	0.4	99.0
SG-09-37 (b)	42.0	2.6	12.2	13.8	13.2	11.3	2.3	0.4	98.0
SG-09-37 (c)	41.5	2.6	12.9	14.4	12.7	11.3	2.4	0.4	98.3
SG-09-37 (d)	40.4	2.4	12.5	14.9	12.5	11.0	2.5	0.4	96.7
SG-09-37 (d)	41.3	2.4	12.2	14.1	12.7	10.9	2.4	0.4	96.8
802-66	41.7	2.5	12.4	13.2	12.8	11.2	2.6	0.4	96.8
1104-67	42.9	2.5	11.8	13.4	13.7	11.0	2.2	0.3	98.2
1104-67	42.5	2.4	12.4	12.3	14.5	11.1	2.8	0.3	98.5
1234-67	43.4	1.9	12.1	15.7	13.2	11.1	2.7	0.4	100.9
1612	43.0	2.1	14.2	13.2	14.1	10.8	2.9	0.3	100.8
1612	41.7	2.6	11.9	12.3	13.9	10.9	2.1	0.3	96.0
1612	42.3	2.3	12.6	13.6	12.9	11.3	2.5	0.3	98.0
2004-69	42.4	2.4	13.1	14.1	13.3	11.7	2.2	0.5	99.8

this may reflect the low abundance of preserved amphibole cores in many of our samples.

Petrologically constrained amphibole crystallization temperatures (~940 to ~980 °C; Fig. 5) overlap with the maximum temperatures measured at the surface of Santiaguito's active vent (850–950 °C; Sahetapy-Engel et al., 2004), suggesting there may be relatively limited cooling of magma during the final stages of ascent at Santiaguito. The range of depths implied for amphibole crystallization (Fig. 5) is consistent with prior suggestions that there may be a large (~80 km<sup>3</sup>) stratified magma storage zone beneath Santiaguito, consisting mainly of intrusive deposits and crystal mush (e.g., Rose, 1987; Conway et al., 1994). We interpret the wide range of depths in Fig. 5a as suggesting that magma ascends slowly enough through this storage zone for phenocrysts to form. There is extensive amphibole crystallization at shallower levels beneath some other dome-forming volcanoes (e.g., Mont Pelée (Martinique), Mount St. Helens (USA), Shiveluch (Kamchatka), Soufrière Hills (Montserrat); Figs. 5b and 6a), in contrast to Santiaguito. This may reflect a lack of significant shallow magma storage at Santiaguito or the relatively high magmatic temperatures, which lead to the instability of amphibole at shallow crustal pressures (e.g., Rutherford and Hill, 1993).

#### 4.1.2. Plagioclase crystal size distribution

Crystal size distribution (CSD) analysis of plagioclase phenocrysts and microlites was used to explore the extent to which non-hydrous phenocryst phases continue to crystallize at shallow levels in the Santiaguito system (Section 4.1.1). Fig. 2 shows that in each sample, plagioclase phenocrysts and microlites form two distinct trends. This suggests there is a change in the crystallization regime beneath Santiaguito. We interpret the phenocrysts as being from a growth-dominated regime within the deeper magma storage zone (e.g., Barclay et al., 1998; Humphreys et al., 2006) and the smaller crystals as resulting from a nucleation-dominated regime (discussed further in Section 4.2.2). Microlite crystallization is typically associated with ascent-related decompression at shallower levels (Cashman and Blundy, 2000). CSD analysis cannot confirm the depth of this change in crystallization regime, nor whether the transition is abrupt or gradual.

## 4.2. Magma ascent

### 4.2.1. Amphibole decomposition

Garcia and Jacobson (1979) used optical microscopy to identify two types of amphibole breakdown rim: “gabbroic” rims of plagioclase, clinopyroxene, orthopyroxene, and magnetite and “black” rims, very fine aggregates of Fe-oxides and pyroxene. Here, we use terminology based on rim textures seen in BSE images, so “gabbroic” and “black” are referred to as “granular” and “symplectic” respectively (Fig. 9).

Granular decomposition has been attributed to water loss during magma ascent, and the width of these rims calibrated experimentally to constrain the ascent rate of magma (Garcia and Jacobson, 1979; Rutherford and Hill, 1993). However, it is now understood that amphibole breakdown may also result from changes in the composition of co-existing vapor phases, the composition and temperature of silicate melt, and the rate of ion exchange between the amphibole crystal and surrounding melt (e.g., Browne and Gardner, 2006). Furthermore, the simple experimental system assumes that depressurization of magma is continuous, steady, and isothermal (Rutherford and Hill, 1993; Browne and Gardner, 2006). Given these significant uncertainties, the results we obtained using the simple experimental calibration of Rutherford and Hill (1993) should be regarded with caution.

Twenty-one of our samples contain partially decayed amphiboles, which indicate ascent rates of 27–84 m h<sup>-1</sup> (1–2 MPa h<sup>-1</sup>) (Table 1), although since our remaining 20 samples contain only relict amphibole, these should be regarded as maxima. Since these are somewhat higher than rates estimated for dome-building phases in other systems (Table 4), it may be that the Rutherford and Hill (1993) calibration is

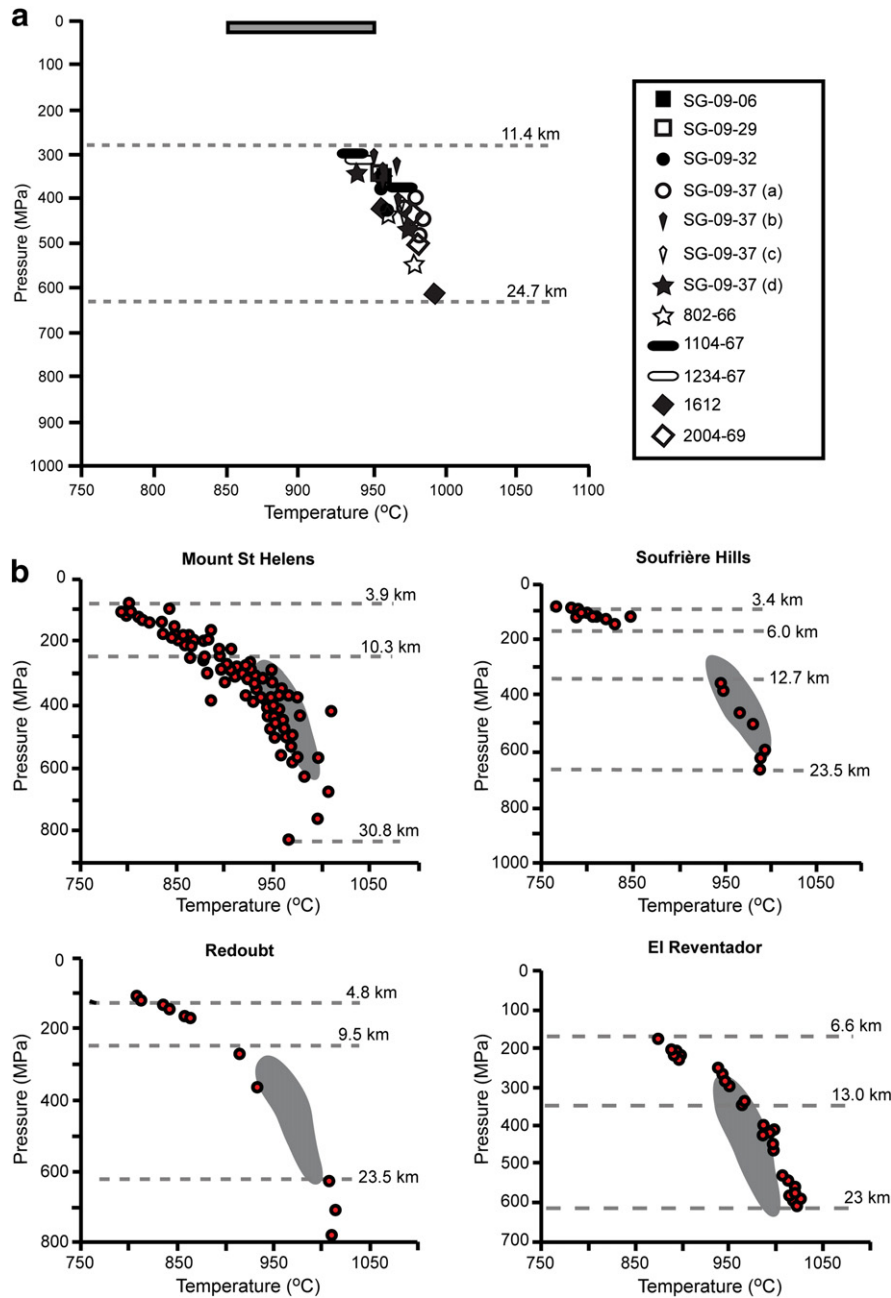


**Fig. 5.** (a) Thermobarometric data for Santiaguito, using the amphibole thermobarometer of [Ridolfi et al. \(2010\)](#). Each symbol represents data from single amphibole phenocrysts; analyses from nine different samples have been included ([Table 2](#)). Analyses of sample SG-09-37 show that considerable variation in depth may be found in amphiboles from the same sample. The gray bar shows the maximum surface temperatures of the Santiaguito vent, measured by [Sahetapy-Engel et al. \(2004\)](#). (b) Data from Mount St. Helens, Soufrière Hills, Redoubt, and El Reventador (slightly modified from [Ridolfi et al., 2010](#)) are plotted for comparison; gray-shaded areas show Santiaguito data.

not be applicable to the Santiaguito system. Each sample contains only one population of rim widths, suggesting there has been minimal mixing between fast- and slow-ascending batches ([Browne and Gardner, 2006](#)). We find no correlation between ascent rate and either age, silica content, or unit type (i.e., dome or flow) ([Table 1](#)); although two of our oldest samples (SG-09-23, SG-09-24) appear to have ascended more slowly than most (27 and 37 m h<sup>-1</sup>). The volume of the Santiaguito complex (~1.1–2 km<sup>3</sup> erupted from 1922 to 2002; [Harris et al., 2003](#); [Durst, 2008](#)) implies an average extrusion rate of 1.4–2.5 × 10<sup>7</sup> m<sup>3</sup> year<sup>-1</sup>. Dividing estimated conduit cross-section (assuming a conduit diameter of 5 to 10 m; [Sahetapy-Engel and Harris, 2009](#)) by the average eruption rate suggests average extrusion rates from the conduit of 20–

145 m h<sup>-1</sup>, broadly consistent with our ascent rates of 27–84 m h<sup>-1</sup> ([Table 1](#)).

#### 4.2.2. Groundmass texture

The slow ascent of viscous, silicic magma, like that of Santiaguito, means the texture of the microlites that crystallize during decompression is often preserved in erupted lava and can be used, along with microlite geochemistry, to assess the ascent path (e.g., [Cashman and Blundy, 2000](#); [Hammer and Rutherford, 2002](#); [Clarke et al., 2007](#)). The Santiaguito microlite population is dominated by plagioclase. Abundant swallowtail and hopper morphologies may be associated with moderate extrusion rates ([Hammer and Rutherford, 2002](#), and references

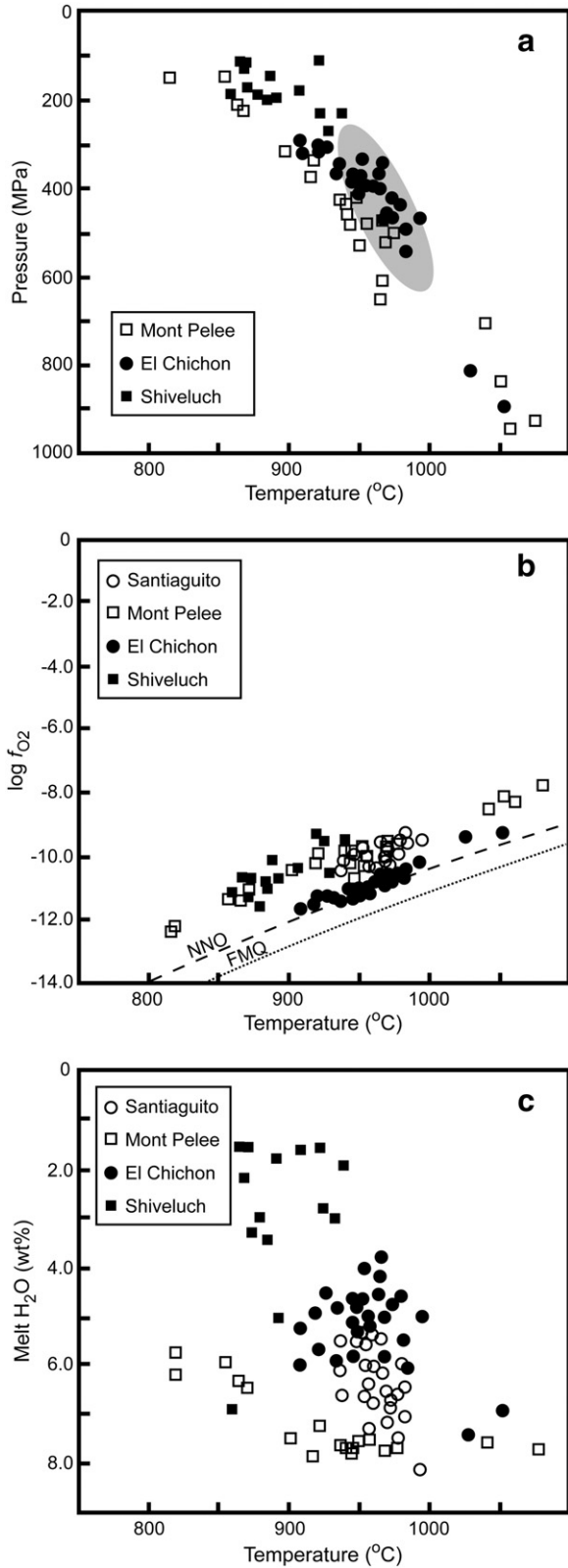


**Fig. 6.** (a) Thermobarometric data, (b) oxygen fugacity, and (c) estimated melt H<sub>2</sub>O concentrations for Santiaguito and three similar dome-forming systems, based on recalculation of published amphibole analyses using the method of Ridolfi et al. (2010). The shaded area in (a) shows the Santiaguito data field for comparison. Bulk rock compositions are trachyandesite (El Chichón) and andesite (Mont Pelée, Shiveluch). References: El Chichón, Andrews et al., 2008; Mont Pelée, Bourdier et al., 1985; Pichavant et al., 2002; Gourgaud et al., 1989; Shiveluch, Kepezhinskas et al., 1997; Taran et al., 1997; Humphreys et al., 2006; all obtained via GEOROC.

therein); their scarcity in our samples is consistent with the comparatively low extrusion rates observed at Santiaguito (measured for flow unit RcM1 as 0.5–1.6 m<sup>3</sup> s<sup>-1</sup> by Harris et al., 2004, compared with up to 20 m<sup>3</sup> s<sup>-1</sup> at Soufrière Hills, Montserrat; Ryan et al., 2010). The average aspect ratio is very low (1.9–3.6), and there is no evidence of the crystal alignment or flow banding described in some domes (e.g., Obsidian Dome, California, USA; Swanson et al., 1989); therefore, the volume% and area% of plagioclase microlites can be assumed equal. The low aspect ratio of plagioclase microlites, and the observed Vulcanian activity and slow extrusion rates at Santiaguito are consistent with slow, multiple-step decompression (as opposed to a single, rapid decompression event; Couch et al., 2003b; Harris et al., 2003; Clarke et al., 2007).

Plagioclase number density ( $N_A$ ) ranges from ~4000 to ~20,000 mm<sup>-2</sup> (Table 3). This value is low, although comparable to the Merapi dome ( $N_A$  ~4000 to ~35,000), and the range is small compared with well-studied, but often more explosive, volcanic systems like Mount St. Helens or Pinatubo (Geschwind and Rutherford, 1995; Hammer et al., 1999, 2000). Plagioclase area fraction ( $\Phi$ , 0.12–0.23) is lower than the 0.4 typical of dome systems (Hammer et al., 2000), suggesting nucleation is more important than growth in the conduit beneath Santiaguito. This is supported by the plot of  $N_A$  vs  $\Phi$  (Fig. 10), which is closer to intersecting the origin (as occurs in ideal experimental cases; Hammer et al., 2000) than on equivalent plots for Merapi (Hammer et al., 2000). The dominance of nucleation over growth is further emphasized by the prominence of small microlite sizes in population density histograms (Supplementary Information Figure D). This may be expected in silicic magma because slow diffusion through increasingly viscous melt may prevent long-distance migration of network-forming ions, inhibiting growth but allowing continued nucleation during the later stages of ascent. A slight displacement of the size distribution peak towards larger crystal sizes in the histograms may indicate ripening in units RcM1, RcM3, RcH, and RcL (exemplified by SG-09-06 from RcH; Supplementary Figure C). Similar displacements found in the population density plots of some older samples (e.g., SG-09-30; Supplementary Figure C) may be due to the exclusion of the smallest microlites, which could not be distinguished from the matrix due to similar total atomic numbers.

Direct observations of effusive flux at Merapi allowed Hammer et al. (2000) to calibrate flux with plagioclase number density and groundmass texture. Unfortunately, a similar relationship cannot be quantified for Santiaguito because the extrusion rates are coarse averages (Harris et al., 2003). Hammer et al. (2000) also found plagioclase  $N_A$  increased with distance from the vent at Merapi, consistent with post-extrusion crystallization. We find no such correlation at Santiaguito, either between different near-vent samples, or between near-vent and flow-tip samples (Fig. 1), which is consistent with the idea that microlite crystallization is inhibited before magma leaves the conduit. The range of pressures over which microlite crystallization ends has previously been called the “final quench pressure” (e.g., Hammer and Rutherford, 2002; Clarke et al., 2007). However, a consideration of the physical state of magma (based on experiments and modelling; e.g., Melnik and Sparks, 1999; Hammer and Rutherford, 2002; Couch et al., 2003b; Clarke et al., 2007; Burgisser et al., 2011) suggests the term “final quench” may be inappropriate. Since the end of crystallization, the preservation of vesicles in the melt, and the transition from ductile to dominantly brittle behavior all occur over a range of pressures, we suggest this region is better described as the “rigidification threshold.” We have used two techniques based on different textural parameters to constrain the location of this threshold quantitatively at Santiaguito.

Hammer and Rutherford (2002) used experimental data to calibrate the relationship between plagioclase morphology and final pressure.

**Table 3**Textural data for Santiaguito groundmass;  $N_A$  is number density (total number of microlites / reference area,  $\text{mm}^{-2}$ );  $\Phi$  is area fraction.

Sample	Glass decay	Plagioclase		Mafics		Vesicles		Area (as solid %)		
		$N_A$	$\Phi$	$N_A$	$\Phi$	$N_A$	$\Phi$	Glass	Plg	Mafics
SG-09-01	No	7590	0.177	28300	0.035	0	0.000	78.8	17.7	3.5
SG-09-03	No	7860	0.179	30440	0.028	1108	0.004	79.2	17.9	2.9
SG-09-04	No	8970	0.219	34260	0.036	134	0.001	74.5	21.9	3.6
SG-09-05	No	6370	0.140	27780	0.032	302	0.002	81.8	14.0	4.3
SG-09-06	No	10520	0.192	37130	0.033	134	0.001	77.5	19.3	3.3
SG-09-07	Yes	5940	0.206	26780	0.032	8493	0.017	75.8	21.0	3.3
SG-09-08	Yes	8410	0.227	31640	0.026	2316	0.006	74.5	22.9	2.6
SG-09-23	Yes	9060	0.225	8760	0.024	0	0.000	72.7	22.5	4.8
SG-09-24	Yes	7530	0.205	16070	0.032	3961	0.029	75.6	21.1	3.3
SG-09-29	Yes	9230	0.199	12020	0.014	4364	0.011	78.5	20.1	1.4
SG-09-30	Yes	8950	0.206	7930	0.028	3458	0.018	76.2	21.0	2.8
SG-09-32	Yes	4150	0.197	16350	0.023	13931	0.039	73.2	21.5	5.3
SG-09-33	Yes	6020	0.160	27410	0.025	15912	0.030	81.0	16.5	2.6
SG-09-34	Yes	6640	0.176	20820	0.034	3223	0.013	78.7	17.9	3.5
SG-09-35	Yes	6820	0.204	18940	0.038	8997	0.036	73.1	21.5	5.4
SG-09-36	No	9520	0.217	8550	0.032	1074	0.003	75.0	21.8	3.2
SG-09-37	No	18090	0.202	18430	0.017	1443	0.011	77.8	20.4	1.8
SG-09-38	No	11320	0.183	10070	0.033	0	0.000	77.3	18.3	4.4
550-67	Yes	7920	0.171	12480	0.022	1477	0.008	80.6	17.2	2.2
802-66	No	12320	0.209	43990	0.038	101	0.000	75.3	20.9	3.8
122967	Yes	9150	0.165	17220	0.021	3156	0.043	80.5	17.3	2.2
123467	No	20950	0.202	45780	0.028	1410	0.008	76.8	20.4	2.9
1510	Yes	7730	0.164	21490	0.040	4163	0.031	78.9	17.0	4.1
1619	Yes	10500	0.190	15370	0.022	839	0.002	78.8	19.0	2.3
2001-69	No	13810	0.197	10220	0.029	739	0.011	77.1	20.0	3.0
2002-69	No	16630	0.214	35740	0.032	1645	0.013	75.1	21.7	3.2
2006-69	Yes	13600	0.180	10410	0.034	201	0.004	75.1	18.1	6.8

Based on their calibrations, the habit and aspect ratio of Santiaguito plagioclase microlites indicate a rigidification pressure of  $\sim 10$  MPa (equivalent to  $\sim 400$  m depth at Santiaguito). Clarke et al. (2007; their Fig. 5) developed an experimental calibration of plagioclase abundance with quench (or rigidification) pressure. Applying this approach to Santiaguito data suggests a pressure of  $\sim 6$  to  $\sim 20$  MPa (equivalent to 200–800 m depth). Based on thermo-acoustic measurements made during a period of explosive and effusive activity, Sahetapy-Engel et al. (2008) suggested the uppermost part of the magma column beneath Santiaguito forms a plug of degassed, viscous silicic magma extending from  $\sim 100$  to  $\sim 600$  m below the surface. Our plagioclase data suggests that the base of this conduit plug or bottleneck may coincide with the magma rigidification threshold.

We have also estimated growth rates for Santiaguito microlites using the area of the largest plagioclase microlites in each sample and the ascent duration (from amphibole rim widths; Section 4.2.1), as demonstrated by Geschwind and Rutherford (1995). The rates obtained for Santiaguito ( $10^{-16}$  m s $^{-1}$ ) are slower than the  $<10^{-13}$  m s $^{-1}$  estimated for the 1980–1986 eruption of Mount St. Helens (Cashman, 1992) and the  $10^{-9}$  to  $10^{-12}$  m s $^{-1}$  calculated during experiments on silicic melt by Hammer and Rutherford (2002).

#### 4.2.3. Vesicle texture

The presence of melt films (Fig. 7d, e) is typical of shallow vesiculation shortly before melt rigidification (Clarke et al., 2007). Preservation of vesicles suggests that degassing was still in progress when melt viscosity became high enough to prevent bubble escape (Section 4.2.2). Although vesicles nucleate and grow in the same way as crystals, albeit much faster, they are more easily destroyed during extrusion (Shea et al., 2010). This may explain why there is no correlation between vesicle number density or area fraction (Table 3) and the matrix glass composition (Supplementary Information Table E). However, a more extensive investigation of vesicle size

distributions may reveal more about the late-stage degassing processes at Santiaguito.

#### 4.2.4. Geochemistry of microlites

The composition of microlites is indistinguishable from that of most phenocrysts (Supplementary Information Table E), implying that microlites began to crystallize from a melt with very similar composition to that which produced the phenocrysts. Plagioclase microlites from Merapi (Fig. 3 of Hammer et al., 2000), Mount St. Helens (Fig. 7 from Cashman, 1992), and Soufrière Hills (Fig. 2 from Humphreys et al., 2009) have distinct and often quite thick ( $>5 \mu\text{m}$ ) rims with lower anorthite content. These rims are generally interpreted as petrological evidence for magma storage in the upper conduit and/or shallow ( $<5$  km depth) storage chamber (e.g., Cashman, 1992; Geschwind and Rutherford, 1995; Hammer et al., 2000; Humphreys et al., 2009). In contrast, zoning in plagioclase microlites from Santiaguito appears absent or barely visible in BSE images, with only occasional, gradual zoning or thin ( $<1 \mu\text{m}$ ) Na-rich rims revealed by element mapping (Supplementary Information Figure C). This means that we have found no petrological evidence for a shallow magma storage chamber at Santiaguito. At Merapi, Mount St. Helens, and Soufrière Hills, petrological interpretations for shallow magma storage have been supported by geophysical data, including seismic and geodetic observations (e.g., Ratdomopurbo and Poupinet, 1995; Musumeci et al., 2002; Paulatto et al., 2012). Similar geophysical investigations are needed at Santiaguito to properly constrain the nature and extent of the shallow plumbing system.

#### 4.2.5. Geochemistry of matrix glass

The experimental calibrations of Hammer and Rutherford (2002) show the normative compositions of Santiaguito matrix glass correlate with rigidification pressure of  $<50$  MPa ( $<2$  km), consistent with estimates based on microlite content and morphology (Section 4.2.2). The pressure experienced by crystallizing magma during ascent can also be constrained by projecting natural glass compositions onto the

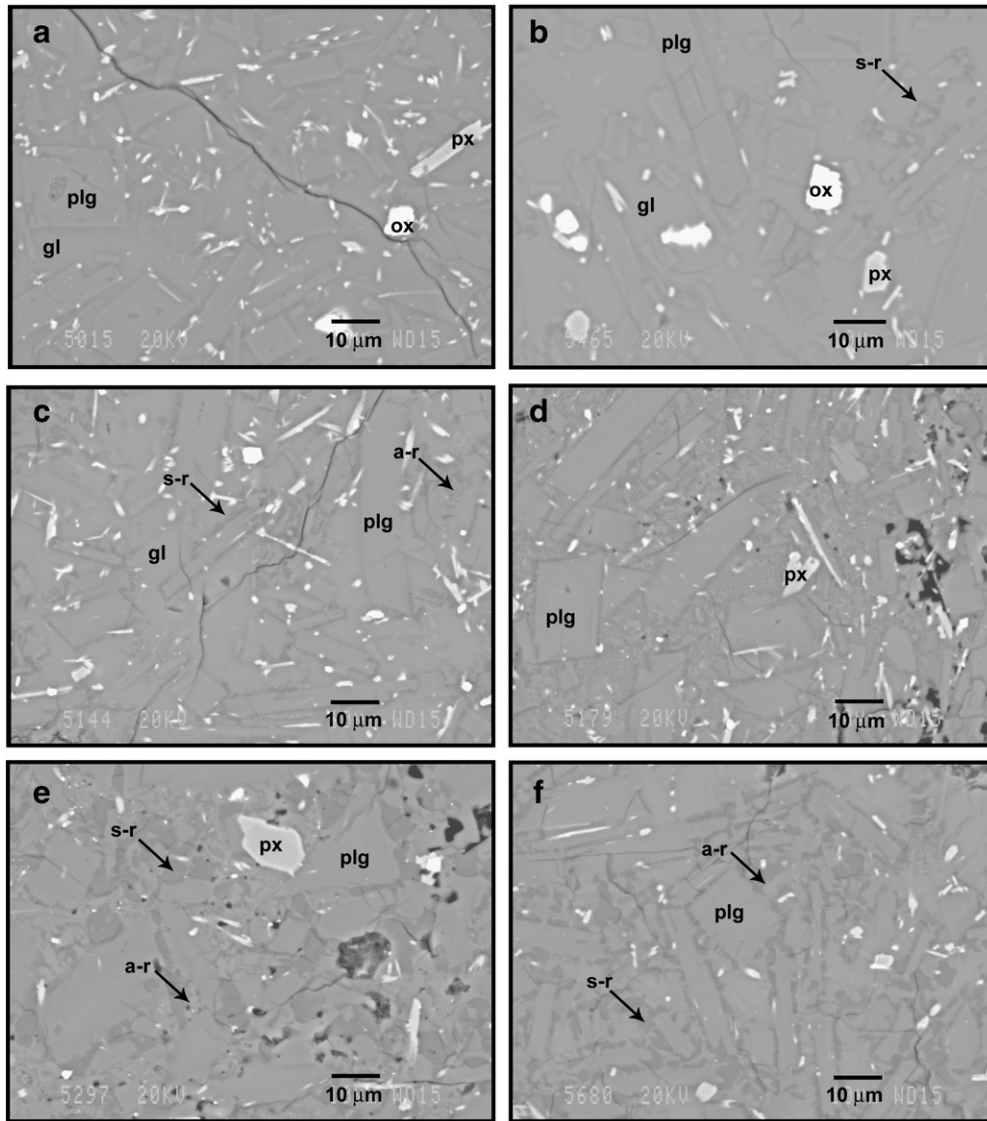


**Fig. 7.** BSE images from different Santiaguito samples, showing progressive breakdown of the matrix glass (gl). In (a), no breakdown has occurred; (b) small, dark gray, silica-rich patches (s-r) are forming around some microlites, particularly in the upper right corner of the image; (c) silica-rich patches are spreading, and now include very small, pale gray streaks of an alkali-rich phase (a-r); (d) silica-rich areas are now widespread and filled with small patches and web-like tendrils of the alkali-rich phase; (e) the fine-scale intergrowths of silica-rich and alkali-rich phases are separating into larger, amorphous patches of each phase – the alkali-rich phase is concentrated around plagioclase microlites, obscuring their original outlines; (f) very few small-scale intergrowths of silica-rich and alkali-rich phases remain.

haplogranite ternary (Qz-Ab-An; Fig. 11), providing geobarometric data independent of amphibole (Blundy and Cashman, 2001, 2008). The results in Fig. 11 are broadly consistent with those discussed in Sections 4.1 and 4.2.2.

### 4.3. Extrusion

#### 4.3.1. Matrix glass

The extent of matrix glass decomposition varies from sample to sample, but together they reveal the progressive nature of glass breakdown at Santiaguito (Fig. 7). Here, pristine glass breaks down via web-like intergrowths, which coarsen and ultimately form patches of crystalline silica (cristobalite) and alkali-rich feldspar (Fig. 7). The fine scale of these initial intergrowths (often  $\ll 0.5 \mu\text{m}$ ), their symplectic texture, and their apparent growth around pre-existing vesicles, suggest glass breakdown occurred when the melt was in a rigid, or near-solid, state.

Devitrification of matrix glass to crystalline silica and alkali feldspar occurs during periods of slow extrusion and in the hot dome

interior at Soufrière Hills (Baxter et al., 1999; Couch et al., 2003a), and experimental investigations of melt decompression have reported crystalline silica forming at high temperatures, but very low pressures (Hammer and Rutherford, 2002; Couch et al., 2003b). Couch et al. (2003b) showed that very slow final ascent, shallow ( $\ll 50$  MPa) stagnation, or shallow stagnation followed by fast final ascent (leaving vesicles in the silica) all resulted in some devitrification. Hammer and Rutherford (2002) found that devitrification did not occur unless the final pressure was  $< 5$  MPa (equivalent to  $< 200$  m depth at Santiaguito); BSE images from the Hammer and Rutherford (2002) experiments clearly show the same, fine-scale, web-like intergrowths found at Santiaguito.

Our observations of the significant variation in glass texture between Santiaguito samples suggests the degree of glass breakdown may depend on extrusion rate – the longer that hot magma is held at low pressure conditions in the uppermost  $< 200$  m of the conduit, the further breakdown progresses. Variations in glass texture between samples taken from the same unit are to be expected, given the variable extrusion rates throughout the lifetime of a unit observed by Harris et al. (2004).

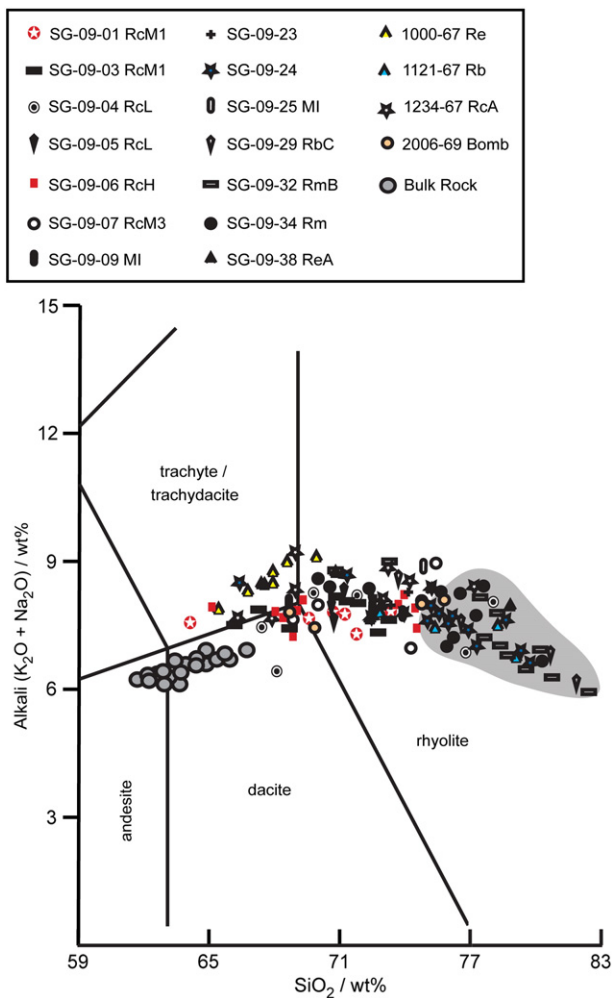


**Fig. 8.** Total alkali–silica plot for Santiaguito glasses and glass decay products; bulk rock analyses from the same samples are shown for comparison (larger filled circles; Scott et al., unpublished data). Data points within the shaded area are heterogeneous due to the glass undergoing fine-scale decomposition to silica-rich and alkali-rich phases.

We find no correlation between the degree of glass breakdown in Santiaguito samples and bulk rock  $\text{SiO}_2$  content, proportion of plagioclase crystals, or matrix glass content. Therefore, we suggest that the extent of glass decay is a qualitative proxy for extrusion rate and we rank our samples by relative extrusion rate in Supplementary Information Table F. These rankings are broadly consistent with ascent rates quantified using amphibole decay rims (Table 1).

#### 4.3.2. Titanomagnetites

Oxyexsolution is a progressive, solid-state reaction of titanomagnetite involving the oxidation of Fe and migration of Ti into thin ilmenite lamellae. Initially, lamellae are restricted to the crystal rims, but if oxidation continues, they may pervade the entire crystal before themselves breaking down to other phases, such as hematite and pseudobrookite (Haggerty, 1991). Oxyexsolution is considered a shallow or surface process because it requires higher oxygen fugacity than experienced during crystallization; crystals must also experience temperatures of at least  $>600^\circ\text{C}$ , for several hours to days (Burton, 1991). In principle, the presence and degree of oxyexsolution may be used to qualitatively constrain the temperature and oxygen fugacity experienced by magma at shallow levels.

Titanomagnetite oxidation does not occur uniformly across a sample — several different stages may be present in a single thin section. This has been observed elsewhere (e.g., Yufu volcano, Japan; Saito et al., 2004) and is most easily explained by heterogeneous oxidation of the melt, perhaps aided by uneven distribution of vesicles within the magma. Oxyexsolution ends as the lava moves away from the hot conduit and cools, explaining why only C1 oxides are present in some units (e.g., if they were extruded rapidly) and why stages C5, C6, and C7 are rare — even slowly extruded magma cools before oxidation can advance this far (Supplementary Information Table F; for definition of stages, see Supplementary Information Table C). Since the conduit walls will be exposed to very high temperatures for a prolonged period, inclusions of wallrock could explain the occasional  $\geq\text{C5}$  oxides in our samples. Using the degree of titanomagnetite oxyexsolution (C1, C2, etc.) as a proxy for extrusion rate allows us to place these samples in rough order of apparent extrusion rate; despite the coarse and qualitative nature of this method, there is some agreement with the rankings based on glass breakdown (Section 4.3.1; Supplementary Information Table F).

#### 4.3.3. Symplectic decay of amphiboles

Since matrix glass and titanomagnetites provided only qualitative proxies for extrusion rate, a third possibility was explored — the symplectic decay of amphibole phenocrysts, which was thought to occur only under highly oxidizing (i.e. shallow) conditions (Garcia and Jacobson, 1979). Symplectic decay is common in Santiaguito amphiboles (Fig. 9), but is usually found as patches between the dominantly granular decay rim and the unaltered phenocryst core. We suggest that formation of a granular rim may temporarily isolate the amphibole phenocryst from the surrounding melt, reducing the diffusive exchange between phenocryst and melt, which makes granular decay possible (e.g., Browne and Gardner, 2006). Under these circumstances, symplectic decay may be the only kinetically possible option, meaning that small symplectic areas are a common, but transient feature of amphibole decay independent of depth or oxygen fugacity. Therefore, while much symplectic decay probably does occur at shallow levels, we do not consider it to be conclusive evidence for shallow alteration of Santiaguito magma.

## 5. Conclusions

Preliminary constraints on the magmatic plumbing system beneath Santiaguito have been obtained using amphibole thermobarometry, phenocryst textures, and the texture and geochemistry of the groundmass (summarized in Fig. 12). However, our data may be naturally biased towards periods of fast lava extrusion, as it is these periods that dominate the sample set.

Amphibole thermobarometry shows that amphibole crystallizes in a continuous storage zone between  $\sim 24$  km and  $\sim 12$  km depth ( $\sim 615$ – $330$  MPa), at temperatures of  $940$ – $980^\circ\text{C}$ , and at oxygen fugacity of  $\log f_{\text{O}_2} - 9.3$  to  $-10.3$ . At other dome-forming systems, amphibole appears to continue crystallizing to shallower depths, which may reflect a lack of significant shallow magma storage at Santiaguito, or the instability of amphibole in Santiaguito magma over  $\sim 900^\circ\text{C}$  at shallow crustal pressures (e.g., Rutherford and Hill, 1993).

Decay rims around amphibole phenocrysts suggest maximum magma ascent rates from  $\sim 12$  km of  $27$ – $84$   $\text{m h}^{-1}$ . Matrix glass composition, microlite habit and aspect ratio, and plagioclase microlites abundances all suggest that ascending melt undergoes rigidification at shallow levels (perhaps between  $\sim 200$  and  $\sim 800$  m). This is consistent with the model of a conduit plug described by Sahetapy-Engel et al. (2008). The preservation of vesicles, the lack of alignment of tabular microlites, the lack of correlation between groundmass textural parameters and distance of the sample from the vent, and the symplectic texture of glass decomposition are also consistent with rigidification prior to extrusion. Finally, matrix glass at Santiaguito undergoes progressive decay in the uppermost

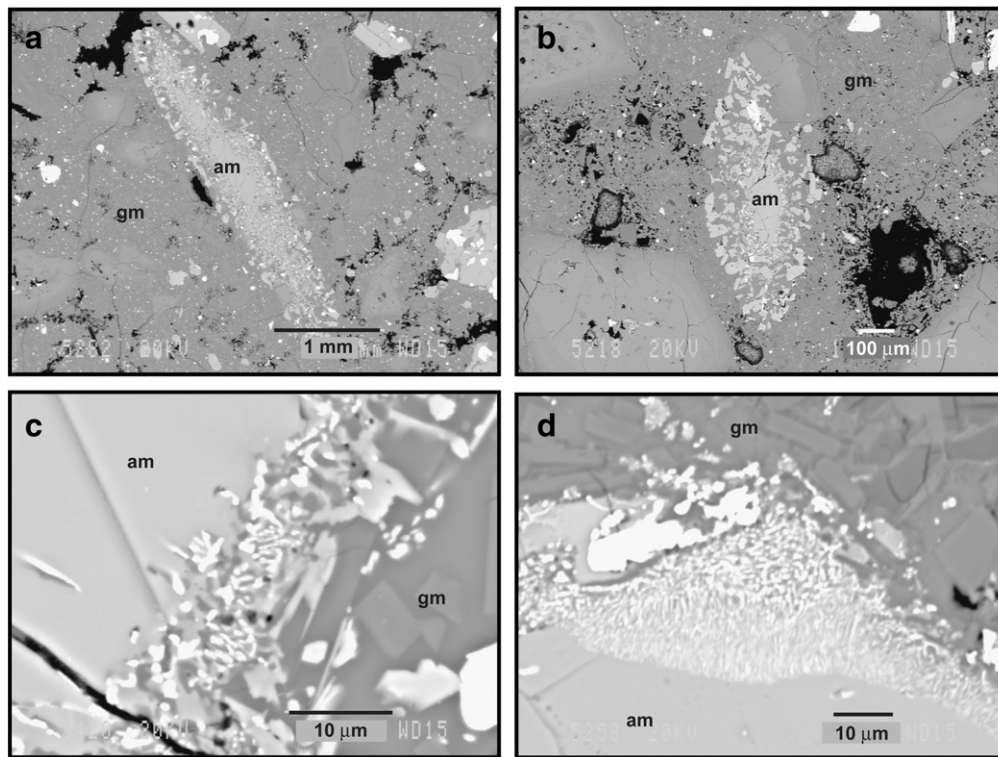


**Fig. 9.** BSE images of amphibole phenocrysts from Santiaguito; am, amphibole; gm, groundmass. (a, b) Typical phenocrysts, with thick granular breakdown rims and small unaltered cores. Breakdown may be symmetric (as shown here) or asymmetric, with significantly thicker rims on one side of the crystal. (c, d) Examples of symplectic decay of amphiboles.

~200 m of the vent before extruding onto the surface as blocky lava. We suggest that experimental calibration of this decay process may provide a quantitative proxy for extrusion rate at Santiaguito.

Our initial petrological results from Santiaguito offer insights into the plumbing of this silicic dome-forming system but raise many further questions that need to be addressed if we are to work towards a broad and more universal understanding of similar systems worldwide and the hazards they represent.

Supplementary data to this article can be found online at <http://dx.doi.org/10.1016/j.jvolgeores.2012.05.014>.

## Acknowledgements

Funding was provided by NERC through PhD studentship NE/G524060/1 and the NCEO Dynamic Earth and Geohazards group. TAM thanks the Royal Society for financial support. Field work was completed with invaluable assistance from Julio Cornejo, Jon Stone, and Matt Watson; activity logs were compiled by the diligent OVSAN staff. Permission to work in Guatemala was granted by INSIVUMEH. We gratefully acknowledge the detailed comments of Margaret T. Mangan and Martin J. Streck, which helped us to improve the manuscript.

**Table 4**

Key properties of the magmatic plumbing systems of Santiaguito (this study) and other subduction zone volcanoes.

			Storage depths (km)	Storage temperatures (°C)	Ascent rate (m h <sup>-1</sup> )	Pre-eruptive H <sub>2</sub> O (wt.%)	log <i>f</i> O <sub>2</sub>
Colima <sup>a</sup>	Mexico	Andesite	1) 2.3 to 6.6	940 to 1060	24 to 38	3.5	−10.5 to −12.2
Mont Pelée <sup>b</sup>	West Indies	Andesite	1) 2.5 to 8 2) <15	821 to 902		1.4 to 5.0	−11.1 to −12.7
Mt St. Helens <sup>c</sup>	USA	Dacite	1) 3.5 to 6 2) 9 to 16	860 to 900	16 to 38	4.5 to 5.5	−10.8
Redoubt <sup>d</sup>	USA	Andesite, dacite	1) 6 to 10	840 to 950	not quantified	4.5	−9.0 to −11.1
Reventador <sup>e</sup>	Ecuador	Andesite	1) 6.5 to 12.5	850 to 1050		~5	~−9 to −12
Santiaguito <sup>f</sup>	Guatemala	Andesite, dacite	1) 12 to 24	938 to 984	50 to 84	5 to 7	−9.3 to −10.3
Shiveluch <sup>g</sup>	Kamchatka	Andesite	1) 5 to 6	840		≤5.1	−9.0 to −10.3
Soufrière Hills <sup>h</sup>	West Indies	Andesite	1) 5 to 6 2) 12.7 to 23.5	1) 820 to 880	4 to 43	4.27 (±0.5)	−11.2 to −11.7
Unzen <sup>i</sup>	Japan	Dacite	1) 3 to 4 2) ~11	900	10 to 26	2 to 5	−10.4 to −12.5

<sup>a</sup> Luhr and Carmichael, 1980; Luhr, 2002.

<sup>b</sup> Gourgaud et al., 1989; Martel et al., 1998.

<sup>c</sup> Cashman, 1992; Rutherford and Hill, 1993; Cashman and McConnell, 2005; Rutherford and Hill, 1993.

<sup>d</sup> Swanson et al., 1994; Wolf and Eichelberger, 1997.

<sup>e</sup> Ridolfi et al., 2008; Samaniego et al., 2008.

<sup>f</sup> This study.

<sup>g</sup> Humphreys et al., 2006, 2008.

<sup>h</sup> Barclay et al., 1998; Devine et al., 1998; Murphy et al., 2000; Ridolfi et al., 2010.

<sup>i</sup> Nakada et al., 1995; Venezky and Rutherford, 1999; Holtz et al., 2005.

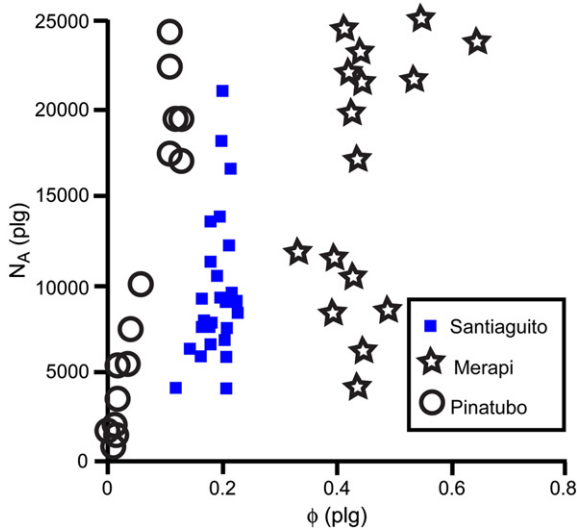


**Fig. 10.**  $N_A$  (number density) vs.  $\Phi$  (area fraction) for plagioclase microlites at Santiaguito (this study) and Merapi domes (Hammer et al., 2000), and Pinatubo surge deposits (Hammer et al., 1999). Most Pinatubo samples have  $N_A$  over 25,000; these are not shown here. The trend for Santiaguito data is fairly close to intersecting the origin, consistent with a nucleation-dominated system.

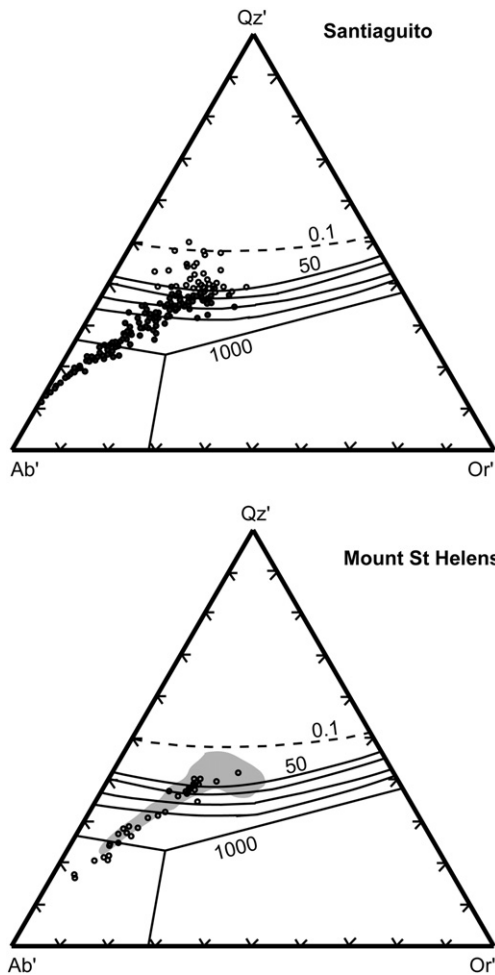


**Fig. 11.** Haplogranite ternary diagrams for glass at Santiaguito (this study) and Mount St. Helens (from Blundy and Cashman, 2001). The Santiaguito data is from analysis of matrix glass; filled circles represent unaltered glass, open circles represent glass decomposition products. The points on the Mount St. Helens ternary are all from melt inclusion glass; the shaded area represents Mount St. Helens matrix glass analyses. Contours represent 0.1, 50, 100, 200, 300, and 1000 MPa.

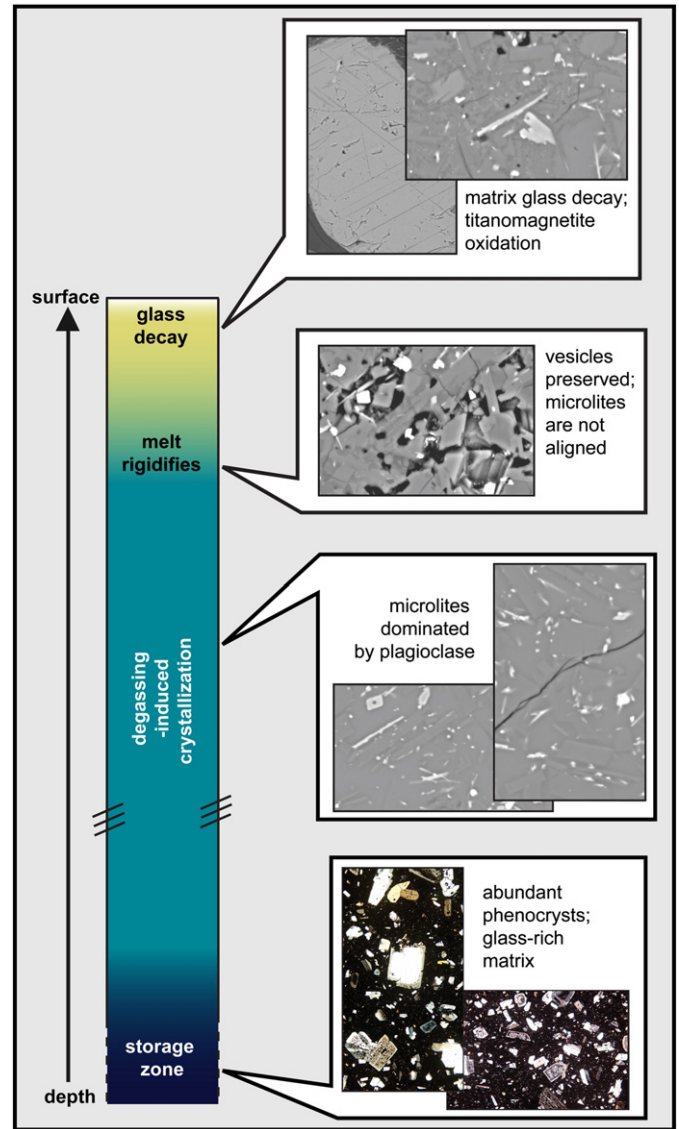


**Fig. 12.** A summary of the magmatic plumbing system beneath Santiaguito. The stages of textural development (phenocryst growth in the storage zone, degassing-induced crystallization, melt rigidification, and matrix glass decay) are shown alongside the petrological evidence for each stage (as discussed in the text).

## References

- Andrews, B.J., Gardner, J.E., Housh, T.B., 2008. Repeated recharge, assimilation, and hybridization in magmas erupted from El Chichón as recorded by plagioclase and amphibole phenocrysts. *Journal of Volcanology and Geothermal Research* 175, 415–426.
- Barclay, J., Rutherford, M.J., Carroll, M.R., Murphy, M.D., Devine, J.D., Gardner, J., Sparks, R.S.J., 1998. Experimental phase equilibria constraints on pre-eruptive storage conditions of the Soufrière Hills magma. *Geophysical Research Letters* 25, 3437–3440.
- Bardintzeff, J.-M., Brousse, R., Clochatti, R., Weiss, J., 1980. Evolution des phénocristaux et de leurs inclusions magmatiques dans la dacite du dome Santiaguito (Guatemala). *Comptes Rendus de l'Académie des Sciences Paris, Série D* 290, 743–746.
- Baxter, P.J., Bonadonna, C., Dupree, R., Hards, V.L., Kohn, S.C., Murphy, M.D., Nichols, A., Nicholson, R.A., Norton, G., Searl, A., Sparks, R.S.J., Vicker, B.P., 1999. Cristobalite in volcanic ash of the Soufrière Hills volcano, Montserrat, British West Indies. *Science* 283, 1142–1145.
- Blundy, J., Cashman, K., 2001. Ascent-driven crystallization of dacite magmas at Mount St. Helens, 1980–1986. *Contributions to Mineralogy and Petrology* 140, 631–650.
- Blundy, J., Cashman, K.V., 2008. Petrologic reconstruction of magmatic system variables and processes. *Reviews in Mineralogy and Geochemistry* 69, 179–239.
- Bluth, G.J.S., Rose, W.I., 2004. Observations of eruptive activity at Santiaguito Volcano, Guatemala. *Journal of Volcanology and Geothermal Research* 136, 297–302.
- Bourdier, J.-L., Gougaud, A., Vincent, P.M., 1985. Magma mixing in a main stage of formation of Montagne Pelée: the Saint Vincent-type scoria flow sequence (Martinique, F.W.I.). *Journal of Volcanology and Geothermal Research* 25, 309–332.

- Browne, B.L., Gardner, J.E., 2006. The influence of magma ascent path on the texture, mineralogy, and formation of hornblende reaction rims. *Earth and Planetary Science Letters* 246, 161–176.
- Burgisser, A., Arbaret, L., Druitt, T.H., Giachetti, T., 2011. Pre-explosive conduit conditions of the 1997 vulcanian explosions at Soufrière Hills volcano, Montserrat: II. Overpressure and depth distributions. *Journal of Volcanology and Geothermal Research* 199, 193–205.
- Burton, B.P., 1991. Interplay of chemical and magnetic ordering. *Reviews in Mineralogy* 5, 303–322.
- Cáceres, D., Monterroso, D., Tavakoli, B., 2005. Crustal deformation in northern Central America. *Tectonophysics* 404, 119–131.
- Carr, M.J., Feigenson, M.D., Bennett, E.A., 1990. Incompatible element and isotopic evidence for tectonic control of source mixing and melt extraction along the Central American arc. *Contributions to Mineralogy and Petrology* 105, 369–380.
- Cashman, K.V., 1992. Groundmass crystallization of Mount St. Helens dacite, 1980–1986: a tool for interpreting shallow magmatic processes. *Contributions to Mineralogy and Petrology* 109, 431–449.
- Cashman, K., Blundy, J., 2000. Degassing and crystallization of ascending andesite and dacite. *Philosophical Transactions of the Royal Society A* 358, 1487–1513.
- Cashman, K.V., McConnell, S.M., 2005. Multiple levels of magma storage during the 1980 summer eruptions of Mount St. Helens, WA. *Bulletin of Volcanology* 68, 57–75.
- Clarke, A.B., Stephens, S., Teasdale, R., Sparks, R.S.J., Diller, K., 2007. Petrologic constraints on the decompression history of magma prior to vulcanian explosions at the Soufrière Hills volcano, Montserrat. *Journal of Volcanology and Geothermal Research* 161, 261–274.
- Conway, F.M., Diehl, J.F., Rose, W.I., Matías, O., 1994. Age and magma flux of Santa Maria volcano, Guatemala: correlation of paleomagnetic waveforms with the 28000 to 25000 yr BP Mono Lake excursion. *Journal of Geology* 102, 11–24.
- Couch, S., Harford, C.L., Sparks, R.S.J., Carroll, M.R., 2003a. Experimental constraints on the conditions of formation of highly calcic plagioclase microclites at the Soufrière Hills volcano, Montserrat. *Journal of Petrology* 44, 1455–1475.
- Couch, S., Sparks, R.S.J., Carroll, M.R., 2003b. The kinetics of degassing-induced crystallization at Soufrière Hills volcano, Montserrat. *Journal of Petrology* 44, 1477–1502.
- Devine, J.D., Rutherford, M.J., Gardner, J.E., 1998. Petrologic determination of ascent rates for the 1995–1997 Soufrière Hills volcano andesitic magma. *Geophysical Research Letters* 25, 3673–3676.
- Durst, K.S., 2008. Erupted magma volume estimates at Santiaguito and Pacaya volcanoes, Guatemala using digital elevation models. M.Sc. Thesis, Michigan Technological University, USA.
- Edmonds, M., Pyle, D., Oppenheimer, C., 2002. HCl emissions at Soufrière Hills Volcano, Montserrat, West Indies, during a second phase of dome-building: November 1999 to October 2000. *Bulletin of Volcanology* 64, 21–30.
- Escobar Wolf, R., Matías Gomez, R.O., Rose, W.I., 2010. Notes on a New Geologic Map of Santiaguito Dome Complex, Guatemala. Geological Society of America Digital Map and Chart Series 8. <http://dx.doi.org/10.1130/2010.DMCH008> (2 pp.).
- García, M.O., Jacobson, S.S., 1979. Crystal clots, amphibole fractionation and the evolution of calc-alkaline magmas. *Contributions to Mineralogy and Petrology* 69, 319–327.
- Geschwind, C.H., Rutherford, M.J., 1995. Crystallization of microclites during magma ascent: the fluid mechanics of the 1980–1986 eruptions at Mount St. Helens. *Bulletin of Volcanology* 57, 356–370.
- Gourgaud, A., Fichaut, M., Joron, J.-L., 1989. Magmatology of Mt Pelée (Martinique, F.W.I.): I: magma mixing and triggering of the 1902 and 1929 Pelean nuées ardentes. *Journal of Volcanology and Geothermal Research* 38, 143–169.
- Haggerty, S.E., 1991. Oxide textures: a mini-atlas. *Reviews in Mineralogy* 5, 129–219.
- Hammer, J.E., Rutherford, M.J., 2002. An experimental study of the kinetics of decompression-induced crystallization in silicic melt. *Journal of Geophysical Research* 107 (B1), 2021.
- Hammer, J.E., Cashman, K.V., Hoblitt, R.P., Newman, S., 1999. Degassing and microclite crystallization during pre-climactic events of the 1991 eruption of Mt Pinatubo, Philippines. *Bulletin of Volcanology* 60, 355–380.
- Hammer, J.E., Cashman, K.V., Voight, B., 2000. Magmatic processes revealed by textural and compositional trends in Merapi dome lavas. *Journal of Volcanology and Geothermal Research* 100, 165–192.
- Harris, A.J.L., Rose, W.I., Flynn, L.P., 2003. Temporal trends in lava dome extrusion at Santiaguito 1922–2000. *Bulletin of Volcanology* 65, 77–89.
- Harris, A.J.L., Flynn, L.P., Matias, O., Rose, W.I., Cornejo, J., 2004. The evolution of an active silicic lava flow field: an ETM+ perspective. *Journal of Volcanology and Geothermal Research* 134, 147–168.
- Helz, R.T., 1979. Alkali exchange between hornblende and melt: a temperature-sensitive reaction. *American Mineralogist* 64, 953–965.
- Higgins, M.D., 2000. Measurement of crystal size distributions. *American Mineralogist* 85, 1105–1116.
- Holland, T., Blundy, J., 1994. Non-ideal interactions in calcic amphiboles and their bearing on amphibole-plagioclase geothermometry. *Contributions to Mineralogy and Petrology* 116, 433–447.
- Holtz, F., Sato, H., Lewis, J., Behrens, H., Nakada, S., 2005. Experimental petrology of the 1991–1995 Unzen dacite, Japan. Part I: phase relations, phase composition and pre-eruptive conditions. *Journal of Petrology* 46, 319–337.
- Humphreys, M.C.S., Blundy, J., Sparks, R.S.J., 2006. Magma evolution and open-system processes at Shiveluch volcano: insights from phenocryst zoning. *Journal of Petrology* 47, 2303–2334.
- Humphreys, M.C.S., Blundy, J.D., Sparks, R.S.J., 2008. Shallow-level decompression crystallisation and deep magma supply at Shiveluch volcano. *Contributions to Mineralogy and Petrology* 155, 45–61.
- Humphreys, M.C.S., Christopher, T., Hards, V., 2009. Microclite transfer by disaggregation of mafic inclusions following magma mixing at Soufrière Hills volcano, Montserrat. *Contributions to Mineralogy and Petrology* 157, 609–624.
- Johnson, M.C., Rutherford, M.J., 1989. Experimental calibration of the aluminium-in-hornblende geobarometer with application to Long Valley caldera (California) volcanic rocks. *Geology* 17, 837–841.
- Kepezhinskas, P.K., McDermott, F., Defant, M.J., Hochstaedter, A.G., Drummond, M.S., Hawkesworth, C.J., Koloskov, A.V., Maury, R.C., Bellon, H., 1997. Trace element and Sr-Nd-Pb isotopic constraints on a three-component model of Kamchatka arc petrogenesis. *Geochimica et Cosmochimica Acta* 61, 577–600.
- Luhr, J.F., 2002. Petrology and geochemistry of the 1991 and 1998–1999 lava flows from Volcán de Colima, México: implications for the end of the current eruptive cycle. *Journal of Volcanology and Geothermal Research* 117, 169–194.
- Luhr, J.F., Carmichael, I.S.E., 1980. The Colima volcanic complex, Mexico. *Contributions to Mineralogy and Petrology* 71, 343–372.
- Martel, C., Pichavant, M., Bourdier, J.-L., Traineau, H., Holtz, F., Scaillet, B., 1998. Magma storage conditions and control of eruption regime in silicic volcanoes: experimental evidence from Mt Pelée. *Earth and Planetary Science Letters* 156, 89–99.
- Melnik, O., Sparks, R.S.J., 1999. Nonlinear dynamics of lava dome extrusion. *Nature* 402, 37–41.
- Murphy, M.D., Sparks, R.S.J., Barclay, J., Carroll, M.R., Brewer, T.S., 2000. Remobilization of andesite magma by intrusion of mafic magma at the Soufrière Hills volcano, Montserrat, West Indies. *Journal of Petrology* 41, 21–42.
- Musumeci, C., Gresta, S., Malone, S.D., 2002. Magma system recharge of Mount St. Helens from precise relative hypocenter location of microearthquakes. *Journal of Geophysical Research* 107, 2264. <http://dx.doi.org/10.1029/2001JB000629>.
- Nakada, S., Motomura, Y., Shimizu, H., 1995. Manner of magma ascent at Unzen volcano (Japan). *Geophysical Research Letters* 22, 567–570.
- Paulatto, M., Annen, C., Henstock, T.J., Kiddle, E., Minshull, T.A., Sparks, R.S.J., Voight, B., 2012. Magma chamber properties from integrated seismic topography and thermal modelling at Montserrat. *Geochemistry, Geophysics, Geosystems* 13, Q01014. <http://dx.doi.org/10.1029/2011GC003892>.
- Pichavant, M., Martel, C., Bourdier, J.-L., Scaillet, B., 2002. Physical conditions, structure, and dynamics of a zoned magma chamber: Mont Pelée (Martinique, Lesser Antilles arc). *Journal of Geophysical Research* B107. <http://dx.doi.org/10.1029/2001JB000315>.
- Ratdomopurbo, A., Poupinet, G., 1995. Monitoring a temporal change of seismic velocity in a volcano: application to the 1992 eruption of Mt. Merapi (Indonesia). *Geophysical Research Letters* 22, 775–778.
- Ridolfi, F., Puerini, M., Renzulli, A., Menna, M., Toulkeridis, T., 2008. The magmatic feeding system of El Reventador volcano (Sub-Andean Zone, Ecuador) constrained by texture, mineralogy and thermobarometry of the 2002 erupted products. *Journal of Volcanology and Geothermal Research* 176, 94–106.
- Ridolfi, F., Renzulli, A., Puerini, M., 2010. Stability and chemical equilibrium of amphibole in calc-alkaline magmas: an overview, new thermobarometric formulations and applications to subduction-related volcanoes. *Contributions to Mineralogy and Petrology* 160, 45–66.
- Rose, W.I., 1972. Santiaguito volcanic dome, Guatemala. *Geological Society of America Bulletin* 83, 1413–1434.
- Rose, W.I., 1987. Santa Maria, Guatemala: bimodal soda-rich calc-alkalic stratovolcano. *Journal of Volcanology and Geothermal Research* 33, 109–129.
- Rutherford, M.J., Devine, J.D., 2003. Magmatic conditions and magma ascent as indicated by hornblende phase equilibria and reactions in the 1995–2002 Soufrière Hills magma. *Journal of Petrology* 44, 1433–1454.
- Rutherford, M.J., Hill, P.M., 1993. Magma ascent rates from amphibole breakdown: an experimental study applied to the 1980–1986 Mount St. Helens eruptions. *Journal of Geophysical Research* 98, 19667–19685.
- Ryan, G.A., Loughlin, S.C., James, M.R., Jones, L.D., Calder, E.S., Christopher, T.C., Strutt, M.H., Wadge, G., 2010. Growth of the lava dome and extrusion rates at Soufrière Hills volcano, Montserrat, West Indies: 2005–2008. *Geophysical Research Letters* 37. <http://dx.doi.org/10.1029/2009GL041477>.
- Sahetapy-Engel, S.T.M., Harris, A.J.L., 2009. Thermal structure and heat loss at the summit crater of an active lava dome. *Bulletin of Volcanology* 71, 15–28.
- Sahetapy-Engel, S.T.M., Flynn, L.P., Harris, A.J.L., 2004. Surface temperature and spectral measurements at Santiaguito lava dome, Guatemala. *Geophysical Research Letters* 31, L19610.
- Sahetapy-Engel, S.T.M., Harris, A.J.L., Marchetti, E., 2008. Thermal, seismic and infrasound observations of persistent explosive activity and conduit dynamics at Santiaguito lava dome, Guatemala. *Journal of Volcanology and Geothermal Research* 173, 1–14.
- Saito, T., Ishikawa, N., Kamata, H., 2004. Iron-titanium oxide minerals in block-and-ash-flow deposits: implications for lava dome oxidation processes. *Journal of Volcanology and Geothermal Research* 138, 283–294.
- Samaniago, P., Eissen, J.-P., Le Pennec, J.-L., Robin, C., Hall, M.L., Mothes, P., Chavrit, D., Cotton, J., 2008. Pre-eruptive physical conditions of El Reventador volcano (Ecuador) inferred from the petrology of the 2002 and 2004–05 eruptions. *Journal of Volcanology and Geothermal Research* 176, 82–93.
- Shea, T., Houghton, B.F., Gurioli, L., Cashman, K.V., Hammer, J.E., Hobden, B.J., 2010. Textural studies of vesicles in volcanic rocks: an integrated methodology. *Journal of Volcanology and Geothermal Research* 190, 271–289.
- Stoiber, R.E., Rose, W.I., 1968. Recent volcanic and fumarolic activity at Santiaguito Volcano, Guatemala. *Bulletin Volcanologique* 33, 475–502.
- Swanson, S.E., Naney, M.T., Westrich, H.R., Eichelberger, J.C., 1989. Crystallization history of the Obsidian Dome, Inyo Domes, California. *Bulletin of Volcanology* 51, 161–176.
- Swanson, S.E., Nye, C.J., Miller, T.P., Avery, V.F., 1994. Geochemistry of the 1989–1990 eruption of Redoubt volcano: Part II. Evidence from mineral and glass chemistry. *Journal of Volcanology and Geothermal Research* 62, 453–468.

- Taran, Y.A., Pokrovskii, B.G., Volynets, O.N., 1997. Hydrogen isotopes in hornblende and biotites from the Quaternary volcanic rocks of the Kamchatka-Kuril arc system. *Geochemistry Journal* 31, 203–221.
- Venezky, D.Y., Rutherford, M.J., 1999. Petrology and Fe-Ti oxide reequilibration of the 1991 Mount Unzen mixed magma. *Journal of Volcanology and Geothermal Research* 89, 213–230.
- Walker, J.A., Patino, L.C., Cameron, B.I., Carr, M.J., 2000. Petrogenetic insights provided by compositional transects across the Central American arc: Southeastern Guatemala and Honduras. *Journal of Geophysical Research* 105, 18949–18963.
- Wolf, K.J., Eichelberger, J.C., 1997. Syneruptive mixing, degassing, and crystallization at Redoubt volcano, eruption of December, 1989 to May, 1990. *Journal of Volcanology and Geothermal Research* 75, 19–37.